UNIVERSITAT DE BARCELONA

A study of the shortwave schemes in the Weather Research and Forecasting model

Alex Montornès Torrecillas

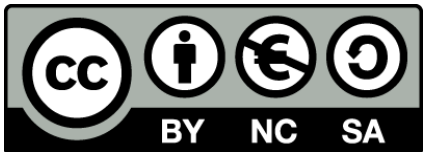

Chapter 3

Description of the solar radiative parameterizations in the WRF-ARW model

3.1 Structure within the WRF-ARW model

3.1.1 Spatial structure of the fields

The WRF-ARW model formulates the Euler equations using a terrain-following hydrostatic-pressure coordinate, η (Skamarock et al., 2008), defined as

$$\eta = \frac{p_h - p_{h,t}}{p_{h,s} - p_{h,t}}, \qquad (3.1)$$

where p_h, $p_{h,t}$ and $p_{h,t}$ are the hydrostatic component of the pressure defined at the current level, at surface and at TOM, respectively. This coordinate is commonly referred as *eta coordinate*.

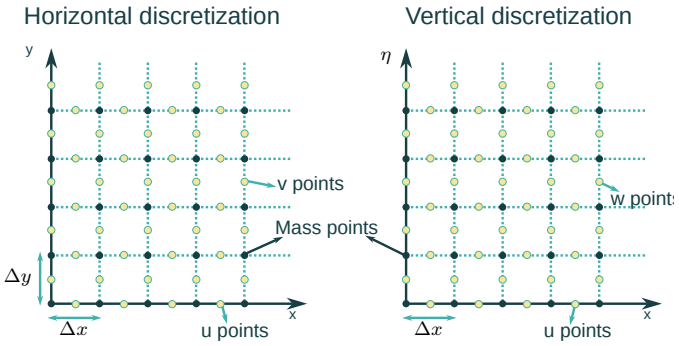

Figure 3.1: Spatial discretization (horizontal and vertical) of the model. Adapted from Skamarock et al. (2008).

The WRF-ARW solver utilizes a C-grid staggering for evaluating the Euler equations (Skamarock et al., 2008). Generally, the thermodynamic variables such as the pressure, air density or humidity, among others, are defined in points denoted as mass points (Fig. 3.1), while the velocities are staggered one half-width with respect to the thermodynamic fields. These points are named u, v and w points, respectively. The geopotential is evaluated at w points.

Typically, the vertical discretization is also referred as full and half levels. Full levels correspond to the w-point levels while the half levels are the mass-point levels. Besides of the thermodynamic variables, the outcomes from

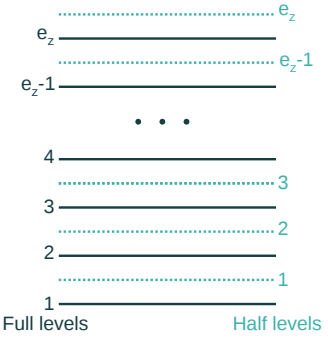

Figure 3.2: Representation of the full and half vertical levels given one grid-point. Figure derived from comments in module_radiation_driver.F

physical parameterizations are determined at half levels, for
this reason, they are also known as physical levels.

The number of vertical levels e_z and the vertical distribution of the η levels can be set by the user in the namelist.input file before running the simulation. The arrays inside the code are indexed from the surface (i.e. k=1, η=1) upward being TOM (i.e. k=e_z, η=0) the last level (Fig. 3.2). By construction, the last half level is fictitious and it does not have data. As we will discuss it in the following chapters, there are some solar schemes that try the opacity between the TOM and the TOA by using the last half level such as a virtual level and extrapolating the information available at TOM. Physically, full levels define the limits between layers while half levels characterizes the properties of the layer.

3.1.2 Model physics

The physical parameterizations of the model are grouped in different drivers. These drivers manage the preprocessing of the outcomes from the dynamic solver, launch the selected packages and perform the postprocessing (if any) prior to returning the information to the main flow of the model.

They are defined by the physical processes represented by the model as: microphysics, deep convection, shallow convection, PBL, surface layer, LSM, surface ocean interactions, radiative transfer (longwave and shortwave), lighting and fire (Table 3.1). The two last ones are not often used WRF-ARW simulations.

Table 3.1: Physical drivers within the WRF-ARW model

Physical processes	Subroutine	Source code
Microphysics	microphysics_driver	phys/module_microphysics_driver.F
Deep convection	cumulus_driver	phys/module_cumulus_driver.F
Shallow convection	shallowcu_driver	phys/module_shallowcu_driver.F
PBL	pbl_driver	phys/module_pbl_driver.F
Surface layer	surface_driver	phys/module_surface_driver.F
LSM	surface_driver	phys/module_surface_driver.F
Surface ocean	ocean_driver	phys/module_sf_ocean_driver.F
Radiation short/longwave	radiation_driver	phys/module_radiation_driver.F
Ligthing	lighting_driver	phys/module_ligthing_driver.F
Fire	fire_driver_em	phys/module_fr_fire_driver.F

With the exception of microphysics, all physical schemes are called in the first part of the Runga-Kutta integration in the following order: i) radiative transfer, ii) surface processes, iii) PBL, d) cumulus (deep and shallow convection) and iv) 3D turbulent kinetic energy (TKE) and vertical/horizontal diffusion.

As it is described in Skamarock et al. (2008), in order to reduce the truncation errors in the calculation of the horizontal pressure gradient as well as the computational rounding errors in the vertical pressure gradient and buoyancy by the dynamic solver, the variables in the Euler equations are expressed as perturbations from a hydrostatically-balanced reference state.

However, the physical parameterizations are designed for working with full physical variables (i.e. perturbed state + reference state) because these fields are more comprehensive

and easy to process. Furthermore, many physical schemes derive from other models and/or from research institutions and thus, the usage of full variables simplify the idea of plug-in modules that can be easily shared within the WRF model community. Therefore, the first step before calling the physical packages is to transform the thermodynamic and dynamic variables evaluated by the dynamic solver into full physical variables consistent with physical parameterizations. This process is performed in a subroutine called phy_prep stored in dyn_em/module_big_step_utilities_em.F.

Furthermore, some physical variables used by the parameterizations must be initialized. This initialization is performed at the beginning of the model execution using the information provided by the namelist.input file. The subroutine that initializes the physics of the model is called phy_init in phys/module_phys_init.F. The treatment is specific for each kind of process. In the case of the radiative transfer there is a routine called ra_init in the same source code file, common for longwave and shortwave radiation.

The part related to the shortwave radiation has a particular routine for each physical option (Table 3.2).

Table 3.2: Initialization of the solar radiative transfer parameterizations.

Solar scheme	Subroutine	Source code
Dudhia	swinit	phys/module_ra_sw.F
Goddard	gsfc_swinit	phys/module_ra_gsfcsw.F
New Goddard	-	-
RRTMG	rrtmg_swinit	phys/module_ra_rrtmg_sw.F
RRTMG-fast	rrtmg_swinit_fast	phys/module_ra_rrtmg_swf.F
CAM	camradinit	phys/module_ra_cam.F
FLG	-	-

3.1.3 Hydrometeors

The determination of the hydrometeors has an important role for the accuracy of the radiative transfer computation in cloudy skies. The physical processes related with the hydrometeors are parameterized in two physical schemes: i) the resolved clouds are considered in the microphysics scheme while ii) the sub-grid contribution is approximated in the cumulus scheme.

In version 3.7.1, the model had 32 microphysics parameterizations with more or less complexity and hence, the type of hydrometeors considered can vary with the set of options selected. Totally, the model can consider 5 species: cloud droplets (i.e. liquid clouds), rain droplets, ice crystals, snow and graupel.

There are two types of microphysics parameterizations. The single-moment schemes that have one prognostic equation for mass per each specie (i.e. mixing ratio) and double-moment schemes that include a prediction equation for the number concentration per each specie.

Generally, solar schemes interact with the mixing ratio because this information is directly compatible for the evaluation of the optical length as described in Sect. 2.5.4. Hereinafter, we will use the following nomenclature: q_c for cloud droplets, q_r for rain, q_i for ice, q_s for snow and q_g for graupel.

3.2 Radiation driver

The radiation driver manages all procedures for running longwave and shortwave parameterizations. These processes can be divided in three stages:

- Preprocessing: prepare all options and fields to be compatible with the radiative parameterizations
- Processing: execute the physical schemes
- Postprocessing: prepare the outcomes to be returned to the main flow

The following discussion is oriented to those aspects that have a direct impact on the evaluation of the radiative transfer in the solar spectral range. Details related with longwave or the post-processing options such as the topography shading are not included here because they are out of the scope of this thesis.

3.2.1 Preprocessing

At this stage the model variables are prepared to be compatible with the specifications of each radiative transfer package. Nevertheless, this process is not well optimized because there are many common processes that could be performed in this part but are performed inside each parameterization. For example, the model arrays are defined from surface upwards as described before. This nomenclature is useless in solar radiative transfer computations because the source of energy (i.e. the Sun) is located at the TOM. Therefore, the first step in all solar schemes is to perform a vertical indexing inversion, increasing the number of code lines free of charge. This could be a point to be improved in the future in order to simplify the code structure. However, it is not a priority now.

Radiative transfer activation

The first step in this process is to check if the radiative transfer must be evaluated at this time step. The activation of the radiative transfer package is controlled by the user with the variable *radt* in the namelist.input file. This variable is domain dependent and the user's guide of the model recommends to set this variable following the rule of 1 minute per kilometer in grid resolution. For example, the optimal value for a domain at 10 km is 10 min. This means that the radiative transfer codes are called every 10 minutes in the simulation time space.

Nevertheless, this parameter can produce some physical inconsistencies. In cloudless situations, *radt* produces step-wise temporal series for the radiative variables (GHI, DHI, DIF) when the history interval is smaller than *radt* because μ_0 is not updated. Ruiz-Arias solved this problem in version 3.5.1 by adding a function that updates the solar surface fluxes when a parameter named *swint_opt* is enabled in the namelist. Another problem occurs in cloudy scenarios. Suppose a grid-point in the aforementioned domain without clouds in the vertical in which the radiative transfer is called at t_0. After three simulation minutes, the microphysics scheme produces a cloud at this grid-point. Then, the solar surface fluxes would not be updated after seven minutes, when the radiative schemes are called again. Therefore, there is a physical inconsistency between microphysics and radiation during 7 minutes.

One solution to this problem is to reduce the parameter *radt*. However, this option increases significantly the computational time of the simulation. As a consequence, it is necessary an agreement between the selection of this parameter and the purposes of the simulation outcomes.

Astronomical variables

The computation of the shortwave radiative transfer requires information regarding to the incoming solar radiation as well as the Sun's position (i.e. declination and μ_0). Solar declination and incoming radiation are computed in terms of the day of the year J and the hour of the day H at the routine *radconst*.

The solar constant is taken as S_0=1370 Wm^{-2} and it is corrected with a factor considering the eccentricity of the Earth, ϵ, following Paltridge and Platt (1976) as

$$\epsilon = 1.000110 + 0.034221\cos(j) + 0.001280\sin(j) + 0.000719\cos(2j) + 0.000077\sin(2j), \quad (3.2)$$

where $j = \frac{360}{365}J$. After examining Eq. 3.2, we found that this factor introduces an annual variation $\sim \pm$2.5% in the incoming radiation with respect to the solar constant. It is negative during the Northern Hemisphere summer and positive during the winter.

Variations in the solar emission due to the Sun activity and cycles are not considered. Nevertheless, the major impact for mesoscale modeling is the 11-y cycle (e.g. wind resource applications). However, this variations are of the order of 0.1% (Haigh, 1999) and hence, they can be neglected.

Moreover, the incoming radiation and the solar declination are returned to the main flow and they are used in other modules as by the surface_driver.

Solar declination is evaluated in terms of the longitude of the Sun from the Vernal Equinox as it is described in many manuals.

Finally, regarding the solar zenith angle, before version 3.5.1, this field was evaluated inside each solar scheme without considering the equation of time correction. From this version, Ruiz-Arias created a new routine named *calc_coszen* that is called by the radiative transfer driver. This routine evaluates μ_0 for each grid-point and it includes the equation of time correction in the astronomy equations.

Solar eclipses

We have been working on including in the model, the variation of the solar radiation at the TOA produced by solar eclipses based on Montornès et al. (2016c). The code can simulate any partial, total or hybrid solar eclipse for the period 1950 to 2050 and is also extensible to a longer period. The algorithm computes analytically the trajectory of the Moon's shadow and the degree of obscuration of the solar disk at each grid-point of the domain based on the Bessel's method and the Five Millennium Catalog of Solar Eclipses provided by NASA, with a negligible computational time. The degree of obscuration is used for modifying the incoming radiation node by node at each radiative call.

This contribution is compatible with the main solar schemes and it can be enabled and disabled by an option in the namelist.input file. The routines related with the solar eclipses are stored in a new module called *phys/module_ra_eclipse.F*. The information about the solar eclipse conditions for each episode is stored in a file called *eclipse_besselian_elements.dat* that must be included in the running folder during the simulation.

At the moment of presenting this thesis, we are in conversations with NCAR for including this contribution.

Cloud fraction

The model evaluates two different cloud fractions depending on the physical schemes: i) the resolved cloud fraction (i.e. microphysics parameterization) and ii) the sub-grid cloud fraction due to the unresolved clouds (i.e. cumulus parameterization).

As mentioned in Sect. 2.5.4, the treatment of the cloud fraction is important for running the cloud overlapping approaches. The total mixing ratios (i.e. resolved + sub-grid) for q_c and q_i are directly the sum of the outcomes provided by microphysics and cumulus schemes. The first guess for the cloud fraction is the product of the cloud fraction provided by both schemes. When the cumulus scheme is disabled, these contributions are disabled.

Cloud fraction is then reevaluated and optimized for radiative transfer computations. There are four different approaches that internally depends on species of hydrometeors evaluated within the microphysics scheme. The method used in the simulation may be selected using the option *icloud* in the namelist.input file.

- For icloud=0, clouds become transparent. This option is not compatible with FLG. Note that this method does not produce the same results than disabling directly the microphysics schemes because the layer with resolved clouds has a higher water vapor concentration than in a completely clear-sky scenario.
- For icloud=1 (by default), the resolved cloud fraction is evaluated following the method proposed by Xu and Randall (1996) and updated by Hong et al. (1998). The set of approximations performed depends on the availability of the hydrometeors species. They can be found in the routine cal_cldfra1 at module_radiation_driver.F.
- For icloud=2, the resolved cloud fraction only can be 0 (cloudless) or 1 (overcast). More information can be found in the routine cal_cldfra2 at module_radiation_driver.F.
- For icloud=3, the model follows the method proposed by Sundqvist et al. (1989) and implemented by Mocko and Cotton (1995). Further details can be found in the routine cal_cldfra3 at module_radiation_driver.F.

  Nevertheless, this option is useless for these schemes that assume binary cloud fraction at each layer, i.e. cloudless or overcast. We do not provide more details regarding these options because it is not in the scope of this chapter.

Aerosols

Solar schemes in the WRF-ARW model use two different approaches for considering the effect of aerosols. On the one hand, some parameterizations such as CAM and FLG have their own data-sets as it will explained in Sects. 3.5 and 3.7. On the other hand, other parameterizations such as RRTMG and New Goddard, among others, can interact with aerosols but this information must be provided externally.

The external information can be derived from the WRF-Chemical (WRF-CHEM) model or it can be provided by the user. The first case is the oldest one and it is compatible with Dudhia, Goddard and RRTMG as it will be explained in respective Sects., 3.3, 3.4 and 3.6. The second case was developed by Ruiz-Arias in version 3.5.1 and it is compatible with New Goddard, RRTMG and RRTMG-fast. This mode is enabled when the namelist.input parameter aer_opt is set to 2.

Under this approach, the user must provide data for the radiative variables of aerosols at 550 nm. This information can be included in the namelist.input file, assuming that they are constant during all the simulation or they can be provided as 2D grids from ancillary files.

In the preprocessing, this method prepares the vertical profiles by assuming rural, urban or maritime aerosols based on a parameter called aer_type defined by the user. The process also infers the spectral information to the respective bands of New Goddard and RRTMG. Further details regarding the treatment of aerosols can be found in module_ra_aerosols.F or in the user's guide.

Since version 3.8, RRTMG can interact also with the aerosols with the option aer_opt=3, by using climatological water and ice processes from the microphysics module.

3.2.2 Processing

At this step the radiative transfer codes for shortwave and longwave regions of the solar spectrum are called. First, the longwave parameterization is launched, and then, the shortwave scheme. Both options are defined by the user using the variables ra_lw_physics and ra_sw_physics in the namelist.input file. Although these variables are domain dependent, it is recommended of using the same configuration at all the nests due to physical consistencies.

At the moment of presenting this thesis, the last release of the model has seven solar schemes (Table 3.3): Dudhia, Goddard, New Goddard, CAM, RRTMG, RRTMG-fast, GDFL, Hurricane WRF Radiation (HWRFA), and FLG. A physical summary the schemes analyzed in this thesis is presented in Fig. 3.3.

GFDL and HWRFRA will not be considered in this document. The first one because it is an old parameterization derived from the ETA level while the second one because it is a version of GFDL oriented to the WRF-Hurricane simulations. GFDL is detailed in Fels and Schwarzkopf (1981).

Table 3.3: Summary of the routines and source code of each solar parameterization.

Solar scheme	Main subroutine	Source code	Discussed
Dudhia	swrad	phys/module_ra_sw.F	Sect. 3.3
Goddard	gsfcswrad	phys/module_ra_gsfcsw.F	Sect. 3.4
New Goddard	goddardrad	phys/module_ra_goddard.F	Sect. 3.4
CAM	camrad	phys/module_ra_cam.F	Sect. 3.5
RRTMG	rrtmg_swrad	phys/module_ra_rrtmg_sw.F	Sect. 3.6
RRTMG fast	rrtmg_swrad_fast	phys/module_ra_rrtmg_swf.F	Sect. 3.6
GFDL	etara	phys/module_ra_gfdleta.F	-
HWRFRA	hwrfra	phys/module_ra_HWRF.F	-
FLG	rad_flg	phys/module_ra_flg.F	Sect. 3.7

3.2.3 Postprocessing

GHI

Although GHI is computed by all schemes as a field referred as downward short wave flux at ground surface, this variable is not returned and it is recomputed in terms of the net short wave flux at ground surface GSW and the albedo α as

$$GHI = \frac{GSW}{1-\alpha}. \tag{3.3}$$

DNI, DHI and DIF

In version 3.5.1, Ruiz-Arias adapted the code for processing the direct and the diffuse irradiances following two approaches:

- For RRTMG and New Goddard, these variables were evaluated directly from the RTE.

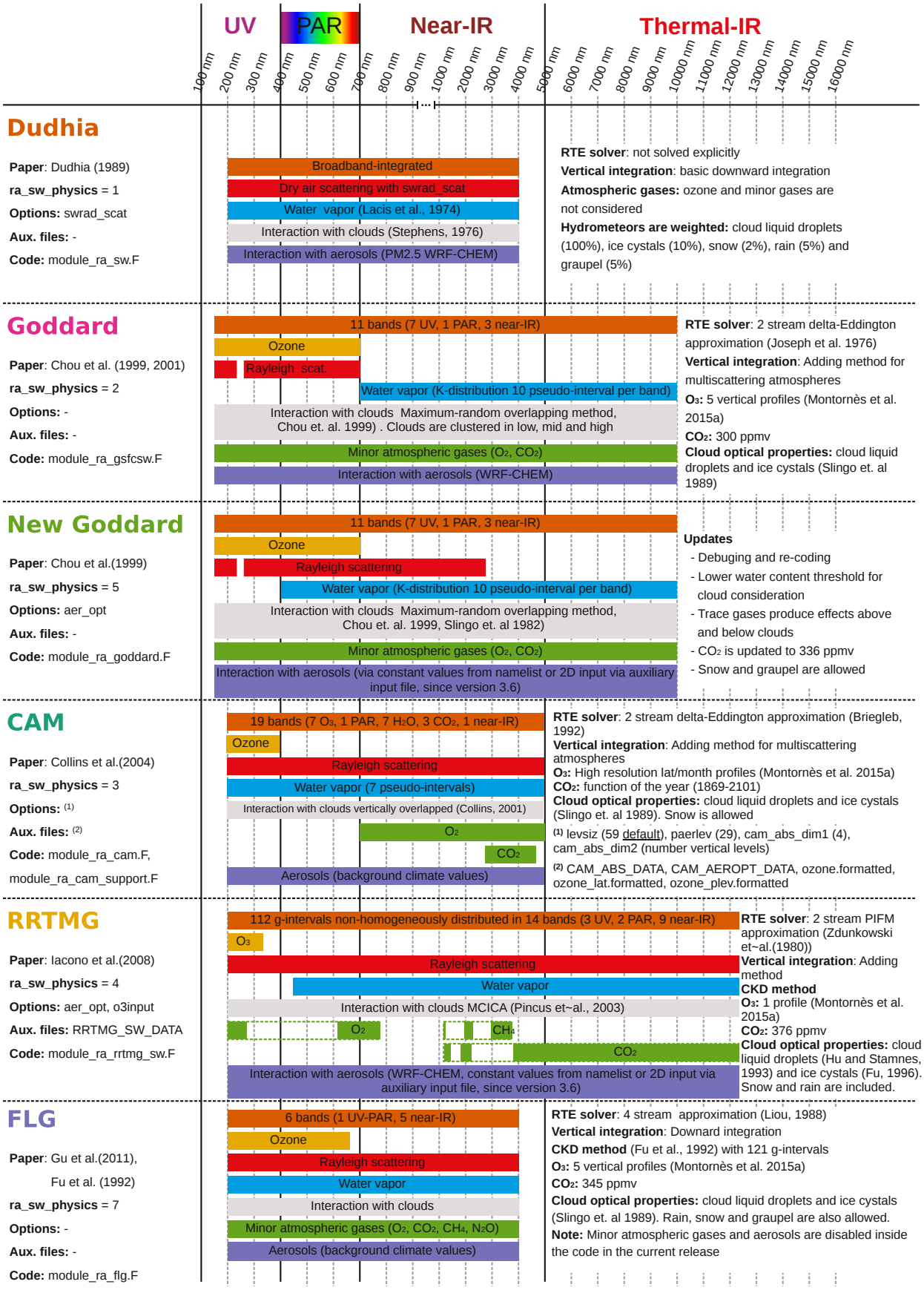

Figure 3.3: Summary of the main physical processes represented for each solar parameterization analyzed in this thesis.

- For the other schemes, these fields were parameterized in terms of the optical air mass and the downward total flux, following Perez et al. (1990), Rigollier et al. (2000) and Ruiz-Arias et al. (2010).

Based on the work developed in this thesis, we extended this implementation to CAM and FLG in version 3.7. This upgrade was not included for Dudhia and Goddard for the following reasons. In Dudhia, this approach has not sense because does not solve the RTE explicitly as we will discuss in Sect. 3.3 and hence, DHI, DNI and DIF are not defined. In Goddard, the code was implemented but was not shared with the user's community because it is an old version of the New Goddard scheme as it will be detailed in Sect. 3.4.

3.3 Dudhia

The scheme proposed by Dudhia (1989) was directly created for the WRF and it is the simplest, fastest and most widely used parameterization in the model. The approach considered in this scheme is simpler than in other parameterizations because the RTE as well as the spectral integration are not solved explicitly. Instead of this, the scheme parameterizes the broadband-integrated attenuation and absorption of the downward flux $F^{\downarrow}$ by including four physical processes in a pseudo-transmissivity: i) dry air clear-sky scattering and attenuation dS_{cs}, ii) water vapor absorption dA_{wv}, iii) cloud absorption dA_{cld} and iv) cloud albedo dR_{cld}.

Following the nomenclature proposed by Dudhia (1989), the downward component of the solar flux $F^{\downarrow}(z)$ at level z is evaluated as

$$F^{\downarrow}(z) = \mu_0 F_{\odot} - \int_{z}^{z_{TOM}} \left(dS_{cs} + dA_{wv} + dA_{cld} + dR_{cld}\right), \tag{3.4}$$

being $\mu_0 F_{\odot}$ the broadband-integrated flux at the TOA.

Eq. 3.4 is computed at each layer for determining the heating rate profile. The downward flux in a layer $z + \Delta z$ is calculated as a function of the previous layer z plus the pseudo-transmissivity of the layer T, i.e.

$$F^{\downarrow}(z + \Delta z) = F^{\downarrow}(z) T(\Delta z), \tag{3.5}$$

where

$$T(\Delta z) = 1 - s_{cs} + a_{wv} + a_{cld} + r_{cld}. \tag{3.6}$$

In Eq. 3.6, the lower case letters correspond to the same physical processes described in Eq. 3.4 but normalized with respect to the flux at the TOA, in this case, integrated from z to $z + \Delta z$. In cases when clouds have a high opacity, the transmissivity can reach zero or near zero values, producing computational problems at the layers below. This issue is solved by defining a minimum value for T of 0.01 and weighting s_{cs}, a_{wv} a_{cld} r_{cld} by a factor S defined as

$$S = \frac{0.99}{s_{cs} + a_{wv} + a_{cld} + r_{cld}}. \tag{3.7}$$

As the vertical component of the solar flux is not considered in this scheme, the heating rate at each layer can not be determined as the divergence of the solar flux given by Eq. 2.40. Consequently, the heating rate at layer Δz must be parameterized as a function of the absorbing terms a_{wv}, a_{cld} and r_{cld} within a layer such as

$$\frac{\partial T}{\partial t} = \frac{1}{\rho c_p \Delta z} \left(a_{wv} + a_{cld} + r_{cld}\right), \tag{3.8}$$

where ρ is the air density in the layer. Note that Eq. 3.8 includes r_{cld} although this term does not represent a real atmospheric absorption.

Dudhia presents two important physical limitations. On the one hand, this scheme does not consider the contribution of O_3 and thus, it should be avoided for simulations with a TOM located above 50 hPa because it can produce problems in the thermal structure of the stratosphere (Montornès et al., 2015e). Moreover, the integral in Eq. 3.4 starts at TOM and thus, the atmosphere between the TOM and the TOA is assumed as transparent for solar radiation. On the other hand, this scheme does not solve the RTE and hence, the direct and diffuse components must be inferred by postprocessing methods as the approach proposed by Ruiz-Arias in version 3.5.1 (Sect. 3.2.3).

The following chapters include more details regarding the methods used for parameterizing each physical process. First, in Sect. 3.3.1, we detail the representation of the dry air scattering and attenuation using a parameter called *swrad_scat* that can be set in the configuration file of the model. In Sect. 3.3.2, the parameterization used for computing the absorption due to water vapor is described. Sect. 3.3.3 considers the set of approaches for including the cloud absorption and reflection. Finally, Sect. 3.3.4 presents a brief description of the aerosol treatment when the WRF-ARW model is coupled with the WRF-CHEM package.

3.3.1 Dry atmosphere

Clear-sky scattering and attenuation are included as a function of a constant C_s and the optical path length of the dry air u_{dry} as

$$s_{cs} = C_s \frac{u_{dry}}{\mu_0}, \tag{3.9}$$

where μ_0 represents the slant path effect.

C_s is defined as

$$C_s = 10^{-5} \text{swrad\_scat } \text{m}^2\text{kg}^{-1}. \tag{3.10}$$

In Eq. 3.10, the variable *swrad_scat* is by default set to 1 and it can be modified by the user in the namelist.input. However, this option is not often used by non-advanced users. The optical path length of the dry air is evaluated as in Eq. 2.140.

Although this term is called *scattering*, it is not a real molecular scattering because it only represents the attenuation of the direct beam but not the increment of the downward flux given by the diffuse component.

3.3.2 Water vapor absorption

The absorption due to water vapor is parameterized using the empirical equation proposed by Lacis and Hansen (1974). In this paper, the authors discussed a relatively fast method for evaluating the solar energy absorbed by the atmosphere. Particularly, Dudhia uses the approach presented for parameterizing the water vapor absorption in cloudless situations.

Before Lacis and Hansen (1974), several authors as Howard et al. (1956) or Yamamoto (1962) performed water vapor absorption measurements in the shortwave spectral region for different values of water vapor amount. Lacis and Hansen fit the Yamamoto's absorption curve for the entire spectrum as

$$a_{wv}(u_{H_2O}) = \frac{2.9 u_{H_2O}}{(1 + 141.5 u_{H_2O})^{0.635} + 5.925 u_{H_2O}}, \tag{3.11}$$

being u_{H_2O} the water vapor amount (in centimeters of precipitable water vapor) and considering standard pressure and temperature conditions (i.e. 1013 hPa and 273 K). In order to apply Eq. 3.11 to any level, they defined an effective u_{H_2O} by using the one-parameter scaling

method (Eq. 2.123). Moreover, as it is described by Lacis and Hansen (1974), Goody (1964) indicated that there is a little theoretical justification for using Eq. 3.11 for the entire spectrum but Lacis and Hansen suggested that it is enough as a first approximation. Finally, Lacis and Hansen (1974) introduced a magnification factor proposed by Rodgers (1967) to take into account the slant path and refraction.

The implementation in Dudhia is slightly different including two significant discrepancies with respect to the original method. First, Eq. 3.11 is directly used without the one-parameter scaling method. Obviously, this introduces a significant error in the determination of a_{wv} with height. However, this error is compensated by the general form of the vertical profile of the water vapor. The second difference is related with the correction proposed by Rodgers (1967). Instead of the magnification factor, Dudhia introduces the effects of the solar position by dividing the water content by μ_0. Thus, Eq. 3.11 is implemented as

$$a_{wv}(u_{H_2O}/\mu_0) = \frac{2.9u_{H_2O}/\mu_0}{(1+141.5u_{H_2O}/\mu_0)^{0.635}+5.925u_{H_2O}/\mu_0}, \tag{3.12}$$

where u_{H_2O} is given by Eq. 2.110.

Fig. 3.4 shows a representation of the water vapor absorption given by Eq. 3.12 for different values of u_{H_2O} and μ_0. As it is expected, the curve increases monotonically with u_{H_2O}. The correction given by $1/\mu_0$ increases the optical path when Sun has a low angle with respect to the horizon (i.e. the effective path length increases). For low water vapor content (i.e. $\sim$0.01 g cm^{-2}), the absorption ranges from 1.6% (when Sun is at Zenith) to 4.7% (when Sun is near to the horizon). By contrast, for high water vapor content (i.e. $\sim$0.10 g cm^{-2}) the absorption ranges between 18% and 28%.

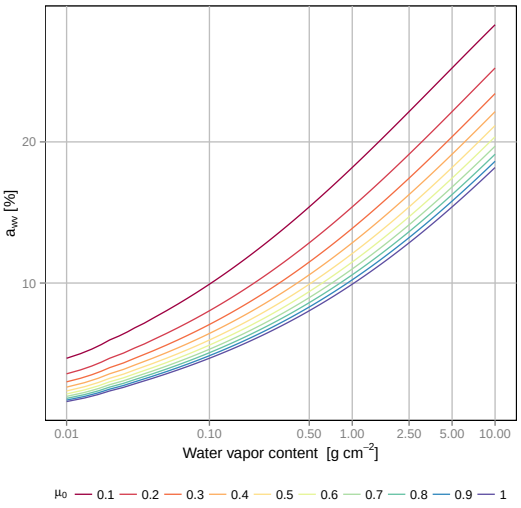

Figure 3.4: Water vapor absorption following Eq. 3.12 and based on Lacis and Hansen (1974).

Note that Eq. 3.12 is defined from TOM to z. Therefore, the absorption a_{wv} produced in a layer between z and $z+\Delta z$ is evaluated as the difference between $a_{wv}(z+\Delta z)$ and $a_{wv}(z)$ and introducing the attenuation produced by the other contributions as

$$a_{wv}(\Delta z) = \big(a_{wv}(z+\Delta z) - a_{wv}(z)\big)\frac{S_0\mu_0 - S_{cs}(z) - A_{cld}(z) - R_{cld}(z)}{S_0\mu_0 - S_{cs}(z) - A_{cld}(z) - R_{cld}(z) - A_{wv}(z)}. \tag{3.13}$$

3.3.3 Clouds

The absorption and reflection by clouds is parameterized in terms of LWC and μ_0. Given a pair of values for LWC and μ_0, the cloud absorption and reflection are evaluated using look-up tables provided by Stephens (1978b) as represented in Fig. 3.5. This paper is the second part of a study composed by three papers: Stephens (1978a), Stephens (1978b) and Stephens et al. (1978).

Basically, Stephens (1978b) proposes a parameterization for shortwave and longwave radiation with the focus on the role of the water clouds. The parameterization is based on a set of eight standard clouds proposed in Stephens (1978a). The transmissivity (i.e. absorption),

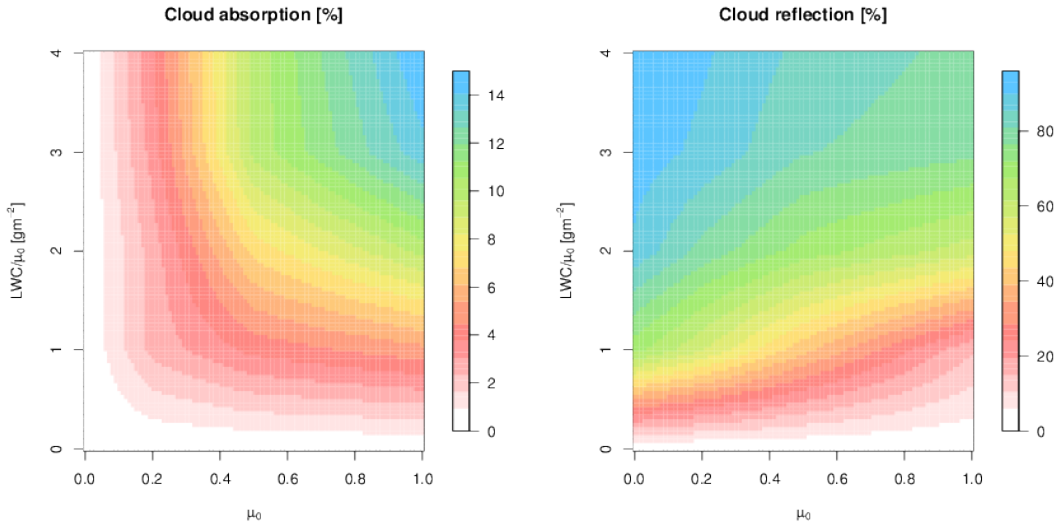

Figure 3.5: Representation of the look-up tables included in Dudhia for cloud absorption (left figure) and reflection (right figure). Both figures are elaborated by using the data-sets provided in the source code, based on Stephens (1978b).

$T_r(\mu_0)$, and the reflectivity (i.e. albedo), $R_e(\mu_0)$, functions of the clouds were evaluated using a multiscattering model proposed by Coakley and Chylek (1975), based on the 2-stream approximation and fully described in Stephens (1978a).

The results were averaged for eight cloud types and for different optical thicknesses (i.e. LWC) as well as μ_0. Finally, the look-up tables shown in Fig. 3.5 were prepared. The absorption by cloud ranges from $<$2% for low LWC and μ_0 values to $\sim$14% for thick clouds and high μ_0 values. The cloud albedo has a high dependence on μ_0. It is minimum when Sun is in the zenith and maximum when it is near to the horizon, reaching values higher than 80% for thin clouds.

The LWC given by Eq. 2.148 is computed using an effective water liquid mixing ratio q^{eff} defined as a composition of all the hydrometeors, i.e.

$$q^{eff} = q_c + 0.1q_i + 0.05q_r + 0.02q_s + 0.05q_g. \tag{3.14}$$

As in the case of the water vapor absorption (Sec. 3.3.2), LWC is corrected by μ_0 in order to consider the slant path. This procedure is not performed in Stephens (1978b) and it could be unnecessary because that parameterization takes into account the effect of the solar position as it is described above.

Finally, given one pair of LWC and μ_0, a_{cld} and r_{cld} are obtained by a linear interpolation. In a similar way that in Eq. 3.13, $a_{cld}(\Delta z)$ and $r_{cld}(\Delta z)$ are determined.

3.3.4 Aerosols

Dudhia is compatible with aerosols when the model is coupled with the WRF-CHEM package. Particularly, this scheme can work with two types of 2.5 μm particles: dry air aerosols and water vapor aerosols.

The implementation of the aerosols is not described in any publication. They are included as a new term in s_{cs} (Eq. 3.9) as

$$s_{cs} = C_s \frac{u_{dry}}{\mu_0} + \frac{\beta \Delta Z}{\mu_0} \left(PM2.5_{dry} + PM2.5_{water}\right) \cdot 5 \cdot 10^{-6}, \tag{3.15}$$

where $PM2.5_{dry}$ and $PM2.5_{water}$ are the particles mass content for both categories and β is a function of μ_0 defined as

$$\beta(\mu_0) = 0.4(1.0 - \mu_0) + 0.1. \tag{3.16}$$

Note that, in the non aerosols case, Eq. 3.15 is reduced to Eq. 3.9. As we will discuss in the following chapters, the parameter C_s can be used as a tuning parameter when aerosols are not considered for reducing the bias in clear-sky conditions.

3.4 Goddard and New Goddard

Goddard and New Goddard are two schemes based on the same publications: Chou and Suarez (1999) and Chou et al. (2001). The second one is an updated version of Goddard with some improvements in the radiative transfer approximation, fixing some bugs and with a process of rewriting the code, being more efficient. Goddard was included in 2000 and New Goddard in 2011, differences between both schemes were fully described in Shi et al. (2011).

This scheme was originally proposed by the NASA Goddard Space Flight Center (GSFC) for being used in global models such as the Goddard Earth Observing System (GEOS) General Circulation Model (GCM), GEOS-GCM, and in limited area models such as the Fifth-Generation Penn State/NCAR Mesoscale Model (MM5). The scheme can deal with shortwave and longwave spectral regions but, in this document, we only will detail the parameterization for solar radiation.

Although the set of approximations are fully detailed in Chou and Suarez (1999) and Chou et al. (2001), both schemes include some modifications with respect to the original publications that will be discussed in the following sections.

3.4.1 Spectral bands

The electromagnetic spectrum is divided into eleven bands: seven in the UV, one in the PAR and three in the near-IR (Table 3.4). For each spectral interval both parameterizations consider the absorption of different gases as well as the Rayleigh scattering.

Absorption due to O_3 is considered in the UV and PAR regions from 0.175 μm to 0.700 μm. The absorption in the band between 0.700 and 1.200 μm proposed in Chou and Suarez (1999) is enhanced in the PAR interval.

The treatment of the water vapor and Rayleigh scattering varies significantly between Goddard and New Goddard. In the first one, the Rayleigh scattering is only evaluated in the UV and PAR regions while the absorption due to H_2O is computed in near-IR bands from 0.700 μm to 10.000 μm . By contrast, New Goddard considers the weak absorption due to water vapor in the PAR band while Rayleigh scattering is included in the first two bands of the near-IR (Fig. 3.3).

Clouds and aerosols are considered for each band in both schemes. As described in Chou and Suarez (1999), the reason for dividing the near-IR region in three different bands is because τ and ω_0 for clouds and aerosols experience a high variation with the wavelength.

Finally, the absorption due to O_2 and CO_2 is considered as a second order contribution. They are included as a reduction of the fluxes with a broadband-integrated parameterization after the spectral integration of the RTE.

3.4.2 Optical properties

Water vapor absorption

The absorption due to H_2O in near-IR bands is evaluated using the k-distribution method (Sect. 2.5.1). Each band is divided in 10 pseudo-intervals in which pseudo-fluxes are evaluated

Table 3.4: Molecular absorption and Rayleigh scattering for each spectral interval in Chou and Suarez (1999), Goddard and New Goddard.

Spectral range [μm]	Chou and Suarez (1999)	Goddard	New Goddard
0.175–0.225	O_3, Rayleigh	O_3, Rayleigh	O_3, Rayleigh
0.225–0.245/0.260-0.280	O_3, Rayleigh	O_3, Rayleigh	O_3, Rayleigh
0.245–0.260	O_3, Rayleigh	O_3, Rayleigh	O_3, Rayleigh
0.280–0.295	O_3, Rayleigh	O_3, Rayleigh	O_3, Rayleigh
0.295–0.310	O_3, Rayleigh	O_3, Rayleigh	O_3, Rayleigh
0.310–0.320	O_3, Rayleigh	O_3, Rayleigh	O_3, Rayleigh
0.320–0.400	O_3, Rayleigh	O_3, Rayleigh	O_3, Rayleigh
0.400–0.700	O_3, Rayleigh,H_2O	O_3, Rayleigh	O_3, Rayleigh,H_2O
0.700–1.220	O_3, Rayleigh,H_2O	H_2O	Rayleigh,H_2O
1.220–2.270	Rayleigh,H_2O	H_2O	Rayleigh,H_2O
2.270–10.000	H_2O	H_2O	H_2O

(Table 2 in Chou and Suarez, 1999). Then, the total flux is calculated as the sum of these fluxes weighted by the k-distribution function.

The k values are defined in a reference state of p_r=300 hPa and T_r=240 K, therefore, u_{H_2O} is scaled following the one-parameter scaling method shown in Eq. 2.123 but with a different temperature scaling function derived from Chou (1986) as

$$u'_{H_2O} = u_{H_2O} \left(\frac{p}{p_r}\right)^{0.8} \big(1 + 0.00135(T - T_r)\big). \tag{3.17}$$

In New Goddard, the absorption due to H_2O in the PAR band is considered using the gray atmosphere approximation with a constant absorption coefficient for the entire band. As it is demonstrated in Chou and Suarez (1999), this approximation is valid because the absorption in the PAR region is weak.

In this case, the mean transmission of the band can be approximated as

$$T_{PAR} \sim \exp(\overline{k} u'_{H_2O}), \tag{3.18}$$

where $\overline{k}$ is an effective absorption coefficient for the whole interval. The $\overline{k}$ values are obtained as

$$\overline{k}(u) = \frac{1}{u} \ln T(u), \tag{3.19}$$

being u the optical length at the reference state given by p_r and T_r.

These coefficients are derived from LBL computations provided by the HITRAN data-set (Sect. 2.5.1), particularly the version of 1996 described in Rothman et al. (1987).

Ozone absorption

As the band intervals defined for the UV and PAR regions are narrow (Table 3.4), the absorption coefficient shows a low variation with λ within the band and the gray atmosphere approximation

can be used. Following Eq. 3.19, the averaged k for each spectral interval is obtained by dividing the eight bands in 127 sub-intervals with a resolution of 0.003 μm and using data provided by WMO (1986), published by the World Meteorological Organization.

As in the case of H_2O, $\overline{k}$ is evaluated at p_r and T_r for a wide range of ozone amounts. Moreover, due to the low dependence of k_{λ,O_3} on pressure and temperature, the one-parameter scaling approximation is neglected in this case. These coefficients are shown in Table 3 of Chou and Suarez (1999). In Goddard, k_{O_3} for the PAR region is considered as 0.0539 (cm–atm)stp^{-1} instead of 0.0572 (cm–atm)stp^{-1} as it was proposed in the original publication and used in New Goddard.

Both schemes include five ozone profiles based on the same data-sets (Fig. 3.6). As it is discussed in Montornès et al. (2015d), these profiles simulate the ozone data for Tropical, Mid-latitude (summer/winter) and Arctic (summer/winter) atmospheres. The selection of the profile to be used in the computations is based on the latitude of the center of the domain as well as on the day of the year. Tropical regions are assumed between 30° S and 30° N without seasonal variation. In this profile, the ozone mixing ratio is maximum at 11.417 hPa with a peak of $1.29{\cdot}10^{-5}$ kg kg^{-1}. Mid-latitudes and Arctic regions are defined between 30–60° and 60–90°, respectively, considering winter and summer variations. In the Northern Hemisphere, winter is assumed between the 285^{th} and the 80^{th} days of the year and summer between the 81^{st} and the 284^{th} day of the year. In the Southern Hemisphere the dates associated with the winter and summer periods are reversed. The ozone layer in Mid-latitudes and Arctic regions has a lower ozone concentration than in the Tropics and is found at a lower altitude in summer than in winter. The highest level for all these profiles is set at 0.0006244 hPa while surface conditions depend on the location and the season.

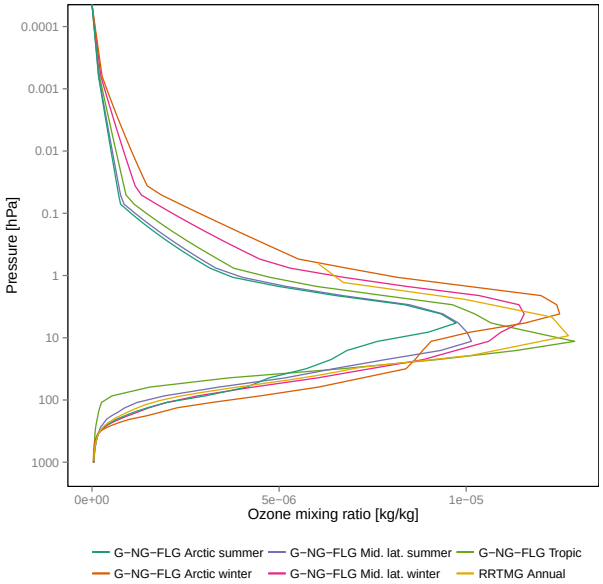

Figure 3.6: Ozone profile data-sets available in the Goddard, New Goddard, FLG and RRTMG parameterizations. Figure extracted from Montornès et al. (2015d).

Oxygen and carbon dioxide absorption

As aforesaid, the absorption by O_2 and CO_2 is considered as a second order contribution and hence, they are not directly included in the RTE evaluation. Instead, their effect is represented as a reduction of the spectral integrated fluxes F (i.e. upward and downward) as

$$F_{red} = F - \Delta F(u_{O_2}) - \Delta F(u_{CO_2}, u_{H_2O}), \tag{3.20}$$

being $\Delta F(u_{O_2})$ and $\Delta F(u_{CO_2}, u_{H_2O})$ the reduction by O_2 and CO_2, respectively, and F_{red} the final flux. Details regarding these parameterizations are fully detailed in Chou and Suarez (1999).

The absorption due to O_2 is parameterized as

$$\Delta F(u_{O_2}) = S_0(1 - \exp(-0.000145 u_{O_2})) \tag{3.21}$$

where 0.000145 $\left((\text{cm-atm})\text{stp}^{-1}\right)^{-1}$ is the averaged absorption coefficient over the entire spectrum and u_{O_2} is the oxygen amount in the layer computed in terms of the mean pressure $\overline{p}$ and μ_0 as

$$u_{O_2} = \frac{165.22}{\mu_0}\left(\frac{\overline{p}}{300}\right)^{0.8}. \tag{3.22}$$

The constant 165.22 is a conversion factor for transforming an atmosphere composed by the 23.14% of O_2 to $(\text{cm-atm})\text{stp}^{-1}$ by assuming standard atmospheric conditions.

CO_2 requires a more complex approach due to the overlapping with water vapor. The flux reduction is considered as

$$\Delta F(u_{CO_2}, u_{H_2O}) = S_0 \Delta T(u_{CO_2}, u_{H_2O}), \tag{3.23}$$

where $\Delta T(u_{CO_2}, u_{H_2O})$ is the reduction transmission function due to CO_2. As it is demonstrated in Chou and Suarez (1999), ΔT depends only on u_{CO_2} and u_{H_2O} and thus, it can be precomputed using the LBL method for a wide range of optical lengths in the Earth atmosphere. These values are provided by the HITRAN data-set (Rothman et al., 1987).

Goddard assumes a single ΔT for the entire spectrum. By contrast, New Goddard uses two ΔT: one representing the weak absorption in the interval from 1.220 to 2.270 μm and the other representing the strong absorption in the last band from 2.270 to 10.000 μm.

The CO_2 mixing ratio q_{CO_2} used for evaluating u_{CO_2} varies from one scheme to the other. In Goddard is set to 300 ppmv, while in New Goddard is updated to 376 ppmv. In a similar way that O_2, u_{CO_2} is determined as

$$u_{CO_2} = \frac{789 q_{CO_2}}{\mu_0}\left(\frac{\overline{p}}{300}\right)^{0.8}, \tag{3.24}$$

where 789 is a conversion factor from ppmv to $(\text{cm-atm})\text{stp}^{-1}$.

Another significant difference between both schemes is that Goddard does not consider the contribution of these gases below clouds.

Rayleigh scattering

For the Rayleigh scattering parameterization both schemes assume the gray atmosphere approximation. The set of extinction coefficients for each spectral interval is determined from the WMO (1986). These values are built in a similar way that in the case of O_3 by following Eq. 3.19. The corresponding values are detailed in Table 3 in Chou and Suarez (1999). The ω_0 and g are considered as 1 and 0, respectively.

Clouds

Goddard and New Goddard use the set of approximations described in Chou and Suarez (1999) but Goddard presents significant simplifications. Moreover, both schemes show differences in the treatment of the hydrometeors.

As it is described in Chou and Suarez (1999), the radiative variables for cloud droplets and ice crystals are evaluated in a similar form that presented in Eqs. 2.152, 2.153 and 2.154. The set of coefficients for evaluating these expressions are presented in Tables 4, 5 and 6 of the same paper and derived from Tsay et al. (1989), for water droplets and from Fu (1996), for ice crystals. Additionally, Chou and Suarez includes the effect of rain particles without considering the dependence on the effective radius.

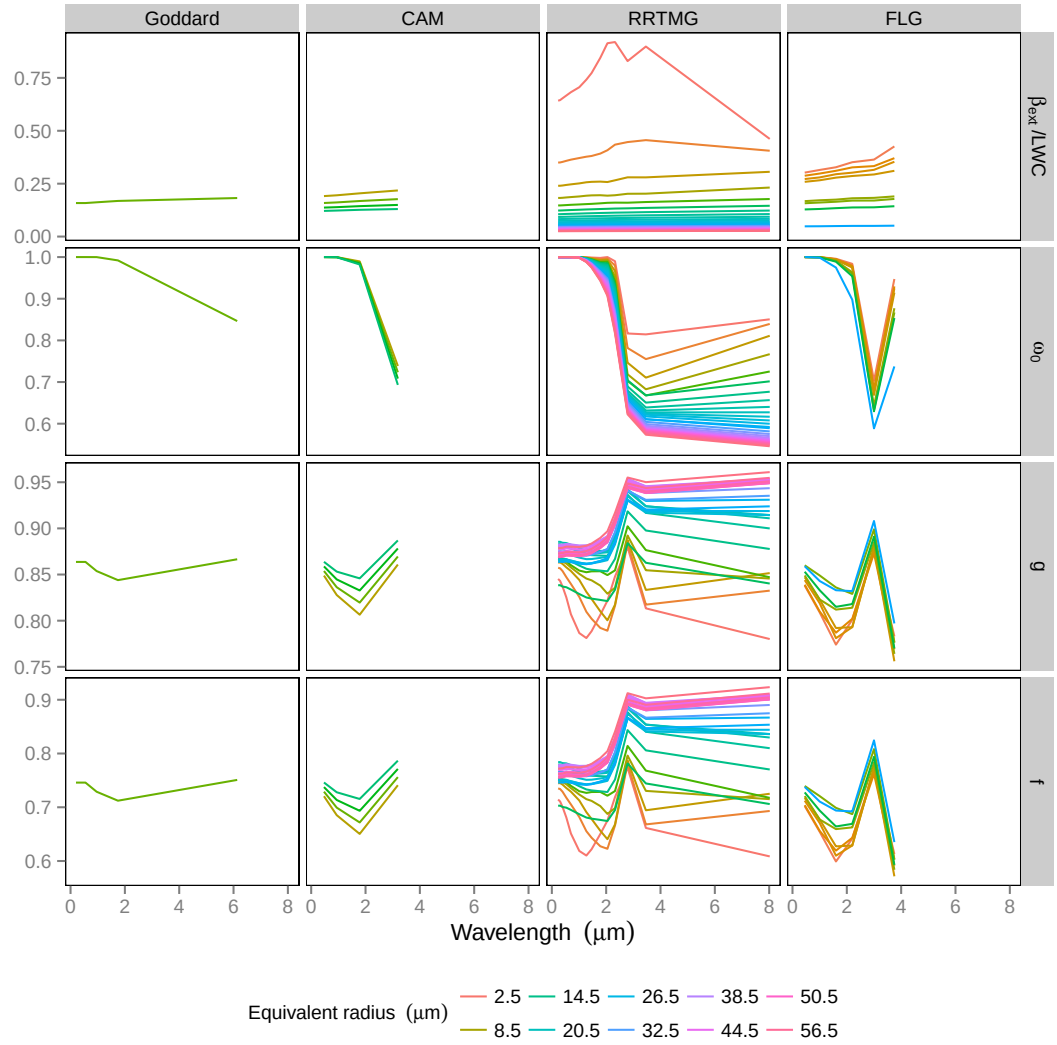

Figure 3.7: Radiative transfer variables for water clouds as a function of the wavelength and $r_{e,l}$. Values are loaded directly from the source codes (Table 3.3). The case of RRTMG is discussed in detail at Sect. 3.6. Goddard includes also New Goddard.

Given the information of each kind of hydrometeor, the composed cloud properties are evaluated as

$$\tau = \tau_l + \tau_i + \tau_r, \tag{3.25}$$

$$\omega_0 = \frac{\omega_{0,l} + \omega_{0,i} + \omega_{0,r}}{\tau} \tag{3.26}$$

and

$$g = \frac{g_l + g_i + g_r}{\omega_{0,l} + \omega_{0,i} + \omega_{0,r}}, \tag{3.27}$$

where indexes l, i and r indicate cloud droplets, ice crystals and rain particles, respectively.

Goddard neglects the contribution of rain particles. The effective radii $r_{e,l}$ and $r_{e,i}$ are assumed as constants with values between 10 μm and 80 μm, respectively. When the WRF-CHEM is coupled to WRF, this scheme can deal with a specie called *Droplet Number* that has

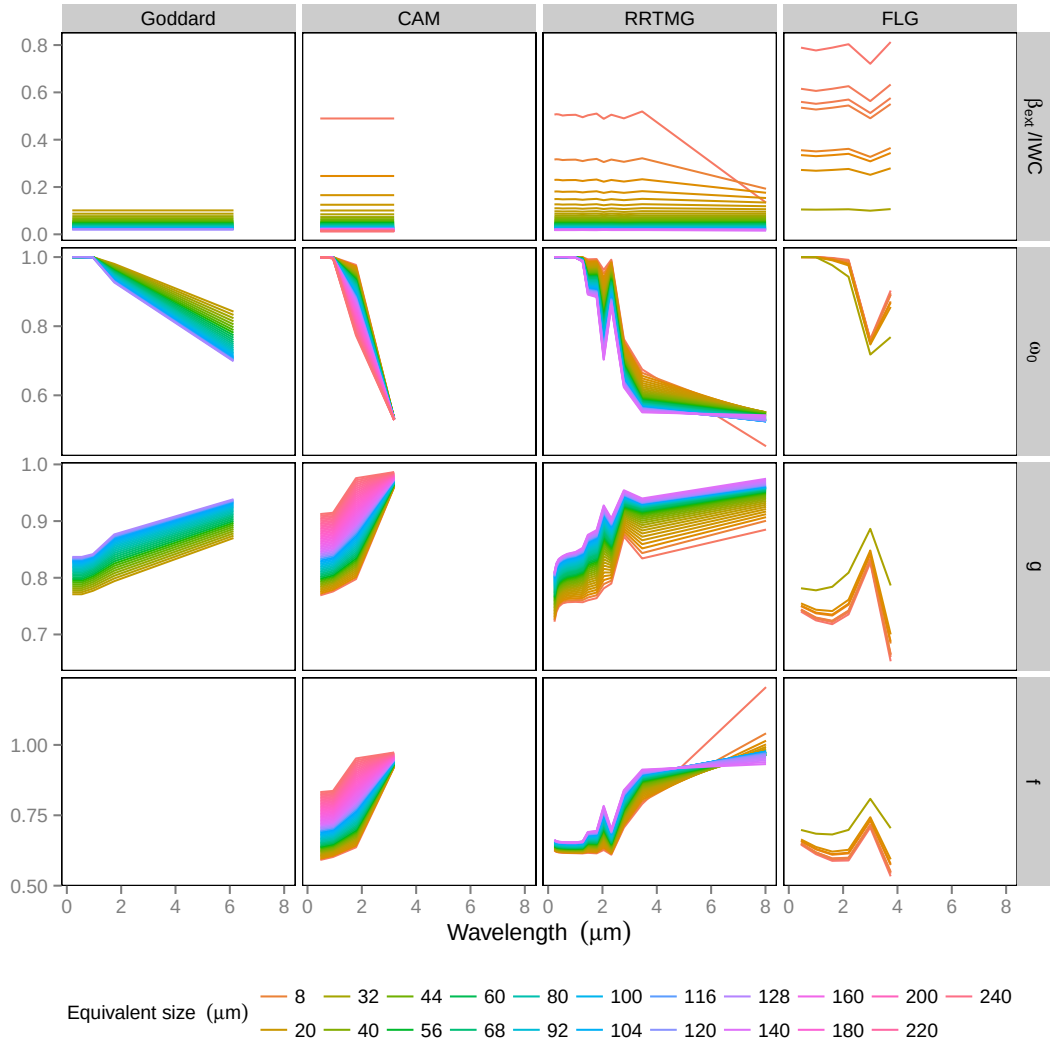

Figure 3.8: Radiative transfer variables for ice clouds as a function of the wavelength and $r_{e,i}$. Values are loaded directly from the source codes (Table 3.3). The case of RRTMG is discussed in detail at Sect. 3.6. As FLG provides the information of the first four expansion coefficients of the phase function, g and f have been computed as $\omega_1/3$ and $\omega_1/5$ based on Eqs. 2.26 and 2.66. Goddard includes also New Goddard.

a specific effective radius equation that substitutes the value for cloud droplets. This approach is rarely used and thus, it is not detailed in this text. The reader can find further details in the source code.

By contrast, New Goddard groups hydrometeors in three categories: cloud water particles (i.e. cloud droplets), cloud ice particles (i.e. ice crystals and snow) and rain particles (i.e. rain droplets and graupel) by summing the respective mixing ratios. For cloud water particles, $r_{e,l}$ is set to 10 μm as in Goddard, while $r_{e,i}$ has a specific equation in terms of the temperature T of the layer given by

$$r_{e,i} = 125 + (T - 243.16)^5. \tag{3.28}$$

This value is limited between 25 and 125 μm.

A representation of the radiative variables for cloud water particles and cloud ice particles can be found in Figs. 3.7 and 3.8.

Another relevant differences between both schemes are in the thresholds for considering cloud layers and in the optimization of the cloud overlapping method.

Regarding the first one, both schemes include clouds based on the composed τ defined in Eq. 3.25 and the cloud fraction of the layer. In Goddard, the threshold for these variables is set to 0.05 and 0.01. Consequently, this scheme can not model the radiative transfer in thin clouds. Conversely, in New Goddard, τ is reduced to 0.0001, improving the accounting for clouds.

In both schemes, the cloud overlapping is treated by using the maximum cloud overlapping approach described in Sect. 2.5.4. Clouds are grouped as high, mid and lower separated by the 400 and 700 hPa levels. The scheme scales τ for the maximum-overlapped clouds within each of the groups.

There is one code option named *overcast* for optimizing the computational costs of the maximum cloud overlapping. This option is oriented to high spatial resolution domains. When it is enabled, the cloud fraction is reduced to 0 (i.e. clear sky) or 1 (overcast). In this case, the scaling of cloud optical thickness is not necessary, reducing the computational resources. When this option is disabled, cloud fraction can take any value between 0 and 1 and hence, the scaling is necessary. Goddard/New Goddard is compiled disabling/enabling this option.

Aerosols

The radiative variables for aerosols are not parameterized and they must be provided from auxiliary data-sets as a function of the grid-point, height and spectral band.

In the case of Goddard, this scheme is compatible with the WRF-CHEM model, particularly, with the Model for Simulating Aerosol Interactions and Chemistry, MOSAIC (Zaveri et al., 2008), module. This module provides the aerosol optical thickness, single-scattering albedo, and asymmetry factor at 300, 400, 600 and 999 nm and then, these values are conformed into the spectral bands used by Goddard.

New Goddard was originally not compatible with aerosols interactions until the modifications introduced by Ruiz-Arias, detailed in Sect. 3.2.1.

Surface albedo

Although both schemes are ready for considering different albedos in the UV-PAR and near-IR spectral regions as well as for direct and diffuse beams, they use always the same value provided by the static data-sets of the model.

3.4.3 Radiative transfer solver

Goddard and New Goddard use the two-stream approach for solving the RTE equation at each layer with the adding method for considering the vertical integration of the fluxes. As it was explained in Shi et al. (2011), New Goddard corrected a bug in the implementation of the adding method included in Goddard.

Regarding the layer between the TOM and the TOA, both schemes introduce a virtual level with a constant temperature and half water mixing ratio and ozone with respect to the TOA.

In both schemes the direct beam transmissivity and reflectivity are computed from the δ-Eddington approach derived from Harshvardhan (1986). Nevertheless, these schemes show significant discrepancies in the implementation of the two-stream approach for the diffuse component of the flux. In Goddard, the diffuse fluxes are obtained following Sagan and Pollack (1967) and Lacis and Hansen (1974). On the contrary, New Goddard follows exhaustively the details provided by Harshvardhan (1986) and Chou and Suarez (1999).

Finally, New Goddard includes a code option called *fast_overcast* that controls the evaluation of the clear-sky fluxes evaluation. When this option is enabled (by default), the code skips the clear-sky radiative transfer calculation, i.e. only cloudy sky fluxes are computed. The code includes a data-set of pre-computed ratios between clear and cloudy fluxes for the flux reduction below clouds due to the trace gases. As it is indicated in phys/module_ra_goddard.F, this option make the radiative scheme faster by 1.5 times introducing an error lower than $1\,\mathrm{Wm}^{-2}$.

3.5 CAM

The CAM solar scheme was originally the shortwave parameterization of the NCAR Community Atmosphere Model, CAM3.0 (Collins et al., 2004). The source code of this scheme was adapted for working with the WRF-ARW model since 2006. The published documentation for this scheme in Collins et al. (2004) is very completed. For this reason, we will present a brief description in this chapter for completeness with the other parameterizations.

3.5.1 Spectral bands

This scheme divides the solar spectrum into 19 spectral and pseudo-spectral intervals in terms of the gases and the physics represented: seven for the O_3, one in the PAR, seven for H_2O, three for CO_2 and one in the near-IR band.

3.5.2 Optical properties

The physical processes represented by this scheme include the absorption by the atmospheric gases (i.e. O_3, H_2O, CO_2 and O_2), the Rayleigh scattering, the absorption/scattering by clouds and the absorption/scattering by aerosols.

Water vapor absorption

The absorption by this gas is treated defining seven pseudo-spectral intervals in the near-IR region. At each one of these intervals, the absorption coefficient is assumed as a constant. The method was proposed by Wiscombe and Evans (1977) and it is basically an exponential-sum fitting of the transmission functions. The conceptual idea is similar that in the CKD method but with a simpler implementation. As detailed in Collins et al. (2004), these coefficients are adjusted to minimize errors in heating rates with respect to LBL calculations at a reference atmosphere.

The water vapor path length is evaluated as the sum of two contributions. On the one hand, the pressure-weighted path following the definition proposed by Collins (2001) as

$$u_{H_2O} = \int_{p_1}^{p_2} \frac{p}{g p_{sfc}} dq_{H_2O}(p) \sim q_{H_2O} \frac{p_2^2 - p_1^2}{2 g p_{sfc}}, \tag{3.29}$$

being p_1 and p_2 the bottom and top pressures of the layer and p_{sfc} the surface pressure.

On the other hand, a contribution for including the stratospheric strong non-overlapping limit derived from Briegleb (1992) as

$$u_{H_2O} = \delta \sqrt{\mu_0 q_{H_2O}} \frac{\Delta p}{g}, \tag{3.30}$$

with δ an empirical factor. In Briegleb (1992), this factor is determined by trial an error being 0.0017. On the contrary, in CAM is optimized for HITRAN and CKD algorithms setting δ to 0.0014257179260883.

Ozone absorption

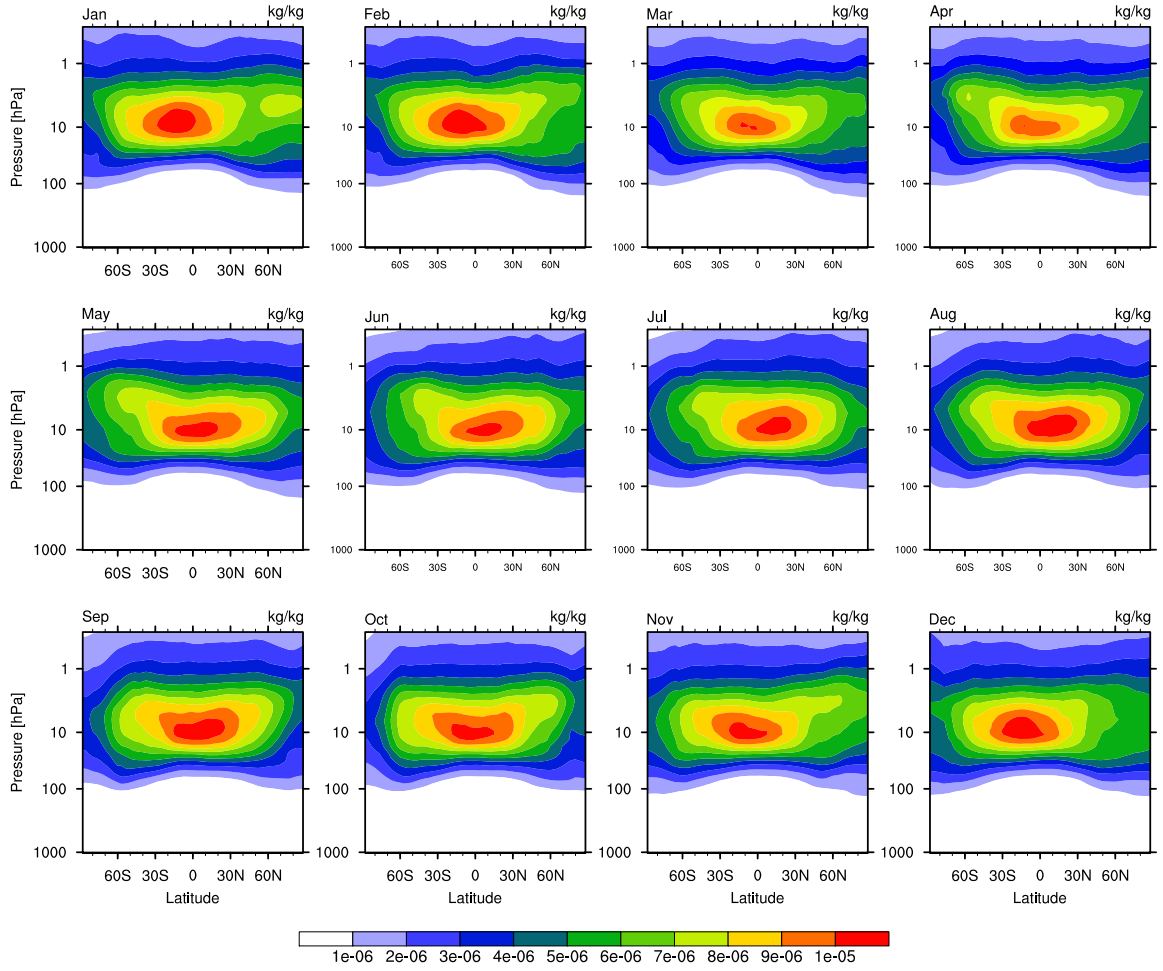

Figure 3.9: Ozone profile data-sets available in the CAM parameterization. Figure extracted from Montornès et al. (2015d).

The ozone absorption is considered over seven interval bands and over the PAR region as well. The scheme assumes the gray atmosphere approximation for each band by defining a constant absorption coefficient at each interval. The procedure used for obtaining these coefficients is detailed in Briegleb (1992) and Collins (1998).

This parameterization includes several ozone profiles as detailed in Montornès et al. (2015d). The data-set covers 64 latitudes with a resolution of $\sim 2.28^{\circ}$ and 59 pressure levels from 1003 to 0.28 hPa for each month of the year (Fig. 3.9). These fields are stored in three binary files: ozone_lat.formatted containing the ozone mixing ratios, ozone_plev.formatted containing the pressure levels and ozone_lat.formatted including the set of latitudes. Ozone values are latitudinally interpolated for each node of the domain.

Oxygen and carbon dioxide absorption

The absorption by O_2 is defined in two spectral intervals: one between 350 nm and 700 nm and the other between 700 nm and 5000 nm. At each one of these bands the optical thickness is computed as $k_{O_2} u_{O_2}$ with and optical depth following the approach of Kiel and Yamanouchi (1985) given by

$$u_{O_2} = \sqrt{\mu_0} q_{O_2} \frac{\Delta p}{g}. \tag{3.31}$$

This implementation is slightly different that the proposed by Briegleb (1992) in which Eq. 3.31 was expressed in terms of $\sqrt{q_{O_2}}$. The oxygen mixing ratio is considered as 0.23143 kgkg^{-1} and the absorption coefficients are taken from Kiel and Yamanouchi (1985) and adjusted for the spectral intervals used in this scheme. Details regarding these coefficients can be found in Table 1a of Briegleb (1992).

The absorption due to CO_2 is considered in two spectral bands. The first one, from 2.630 to 2.860 μm and, the second one, from 4.160 to 4550 μm. This second spectral band is considered as two pseudo-intervals. The treatment of CO_2 is the same that as O_2 with absorption coefficients derived from Kiehl and Ramanathan (1983). The optical length u_{CO_2} is evaluated as in Eq. 3.31 but including $\sqrt{q_{CO_2}}$.

The parameterization has a database for CO_2 concentration since 1869 to 2101 based on the A2 scenario used in the Intergovernmental Panel on Climate Change (IPCC) report (Sankovski et al., 2000). The absorption coefficients are presented in Table 1b of Briegleb (1992) following a the same method than for O_2.

Rayleigh scattering

The Rayleigh extinction coefficients are defined at each band and pseudo-band. These values are taken from Table 1a in Briegleb (1992). The τ is calculated following following Eq. 2.111 while ω_0, g and f are considered as 0.999999, 0 and 1, respectively, for all the intervals.

Clouds

CAM distinguishes the effective radius for water clouds diagnosed over sea, land and sea ice surfaces following the method described by Kiehl et al. (1994). The implementation is different that the proposed in Collins et al. (2004).

The effective radius for cloud droplets is parameterized in terms of the layer temperature, the snow depth, the land/ocean category and the sea ice fraction in four steps:

- First, $r_{e,l}$ is computed over continental surfaces as

$$r'''_{e,l} = 8 + 6\min\big(0, 0.05(273.16 - T)\big). \tag{3.32}$$

- Second, this value is modified introducing the snow depth H_{snow} over land as

$$r''_{e,l} = r'''_{e,l} + (14 - r'''_{e,l})\min\big(1, \max(0, 10H_{snow})\big). \tag{3.33}$$

- Third, the value over land is modified the clean air over ocean by

$$r'_{e,l} = r''_{e,l} + (14 - r''_{e,l})\min\big(1, \max(0, 1 - F_{land})\big). \tag{3.34}$$

- Finally, the algorithm introduces a correction with the presence of ice at surface as

$$r_{e,l} = r'_{e,l} + (14 - r'_{e,l})\min\big(1, \max(0, 1 - F_{ice})\big). \tag{3.35}$$

The effective radius for ice crystals is defined as a function of the temperature following the relationships proposed by Kristjánsson et al. (2000). These values are stored in a pre-computed look-up table ranging from 5.9 μm to 250.6 μm representing the effective ice crystals size between 180 and 274 K. At each layer, $r_{e,i}$ is determined by a linear interpolation.

The radiative variables of clouds are evaluated following Eqs. 2.152, 2.153 and 2.154 but neglecting the quadratic dependence on r_e. The forward scattering fraction necessary for δ-scaling the radiative variables is computed as g^2.

The set of coefficients required for computing those expressions are taken from Slingo (1989) in the case of water clouds and from Ebert and Curry (1992) for ice clouds. Figs. 3.7 and 3.8 show the variation of radiative variables as a function of the effective radius and wavelength.

The treatment of the cloud overlapping is based on the maximum cloud overlapping method following the implementation proposed by Collins (2001). Clouds are grouped as high, mid and low setting as boundaries the level of 400 and 700 hPa.

Aerosols

The CAM parameterization includes a set of interesting routines for considering aerosol direct and indirect feedback during the radiative transfer evaluation based on the considerations explained in Collins et al. (2004). Nevertheless, all this power is not used in practice because the scheme reduces the aerosol data-sets to uniform background aerosol distribution both space and time.

Aerosols are initialized in a routine called aerosol_init that contains the background data-sets. These data-sets are stored in terms of 29 hybrid vertical levels. The optical properties of the aerosol species are stores in an external file called CAM_AEROPT_DATA.

During the code execution, these background profiles are interpolated to the model levels and included in the calculation of the radiative transfer.

Surface albedo

The surface albedo can be specified for the direct and diffuse components in two spectral intervals: one from 200 nm to 700 nm and the other from 700 nm to 5000 nm. Nevertheless, this capability is not used in the WRF-ARW model and the albedo provided by the geographic data-set is assumed for both variables and spectral intervals.

3.5.3 Radiative transfer solver

The reflectivity and transmissivity are evaluated at each layer by using the δ-Eddington approximation following the implementation proposed by Briegleb (1992) and based on Joseph et al. (1976) and Coakley et al. (1983). The multiscattering processes in nonhomogeneous atmospheres are considered using the adding method for the vertical integration of the fluxes.

The scheme assumes a virtual layer between the TOM and the TOA. At this layer, the optical path of the atmospheric gases is evaluated as described above but assuming a constant mixing ratio with respect to the value at the TOM. Aerosols and clouds are not allowed to exist.

As it is described in Collins et al. (2004), the code is optimized for reducing the number of computation in the adding method and for reducing the number of cloud configurations in the maximum cloud overlapping method. Details regarding these features can be found in the literature but they are irrelevant for the discussion presented in this thesis.

3.6 RRTMG and RRTMG-fast

The radiative transfer treatment in the RRTMG parameterization is the most complex of all schemes available in the WRF-ARW model. The fundamentals of this scheme are fully described in Iacono et al. (2008).

The source code is based on the radiative transfer codes developed by the Atmospheric and Environmental Research (AER). The AER group has developed different radiative transfer models that are used in many atmospheric applications as it is described in Clough et al. (2005): remote sensing (e.g. the Technology Experiment Satellite, TES or the Infrared Atmospheric

Sounding Interferometer, IASI), NWP models (e.g. ERA-40, GFS, WRF, Meso-NH, MM5) and climate models (e.g. ECHAM5).

Some of the models developed by the AER group are the LBL Radiative Transfer Model (LBLRTM), the longwave and shortwave Rapid Radiative Transfer Model (RRTM) and, particularly, the longwave and shortwave RRTMG that it is an accelerated version of the RRTM and it will be described in the following sections.

The documentation of the RRTMG in the longwave region is relatively large. However, the information regarding the set of approximations used for the shortwave range is more limited. Consequently, most of the description presented in the following chapters has been directly derived from the source code.

3.6.1 Spectral bands

This scheme divides the solar spectrum in 14 spectral bands. For each band, the molecular absorption is computed using the CKD method based on the outcomes derived from the LBLRTM model as described in Mlawer et al. (1997). In total 112 g-intervals are non-uniformly distributed covering all bands (Table 3.5).

The method for selecting the band intervals is described in Mlawer et al. (1997) for the case of the longwave spectral range. Basically, two criteria are followed, first, each band must represent two absorbing species at the least and, second, the number of spectral intervals must be the minimum as possible.

Under these conditions, species with a significant impact in the absorption of a band are named key species and their contribution to the radiative transfer is considered with many detail. By contrast, those species with a lower impact but non-negligible effects are named minor species and their contribution is parameterized with lower efforts.

Due to the variability of the atmospheric gasses with height, key species at each spectral interval are defined in two different atmospheric regions: lower and upper atmosphere. The boundary between both regions is set in a level where both key species have a low effect in order to minimize the errors due to the transition. This region is chosen at 100 hPa, near to the tropopause, for all the spectral bands (Table 3.5). Consequently, for most of the mesoscale applications, the upper atmosphere species have a low contribution because the TOM is often set between 100 and 10 hPa.

3.6.2 Optical properties

Atmospheric gases

As presented in Sect. 3.6.1, this scheme uses CKD method for considering the dependence of the absorption coefficient with the wavelength. The set of line absorption coefficients are stored in a file named RRTMG_SW_DATA. These values are provided at a set of reference pressure and temperature values: 59 pressure levels from 1050 to 0.01 hPa and 5 temperature values T_{ref}, T_{ref} $\pm$15 K, T_{ref} $\pm$30 K, where T_{ref} at each pressure levels corresponds to the temperature profile at mid-latitudes in summer.

The overlapping of key species is considered defining a magnitude called *binary species parameter* η expressed as

$$\eta = \frac{S_1 u_1}{S_1 U_1 + S_2 u_2} \tag{3.36}$$

where S_1 and S_2 are the integrated line strength for each specie while u_1 and u_2 are the specie amount (i.e. optical length) in the atmospheric column. Eq. 3.36 indicates that, when the first specie is dominant in radiative terms, $\eta \to 1$. On the contrary, when the second one is the dominant, $\eta \to 0$.

Table 3.5: Summary of the g-point values and the key and minor species used at each spectral band. Table derived from the source code. O_2^* indicates absorption in the continuum region

		Lower	atm.	Upper	atm.
Spectral range [μm]	g-points	Key	Minor	Key	Minor
0.200–0.263	6	O_3, O_2	-	O_3, O_2	-
0.263–0.345	8	O_3	-	O_3	-
0.345–0.422	6	-	-	-	-
0.442–0.625	6	H_2O	O_3	-	O_3
0.625–0.778	8	H_2O, O_2	-	O_2	-
0.778–1.242	10	H_2O	-	-	-
1.242–1.299	2	H_2O, O_2	O_2^*	O_2	-
1.299–1.626	10	H_2O, CO_2	-	H_2O, CO_2	-
1.626–1.942	10	H_2O	CH_4	H_2O	CH_4
1.942–2.151	8	H_2O, CO_2	-	H_2O, CO_2	-
2.151–2.500	8	H_2O, CH_4	-	CH_4	-
2.500–3.077	12	H_2O, CO_2	-	H_2O, CO_2	-
3.077–3.846	6	H_2O, CH_4	-	CH_4	-
3.846–12.195	12	H_2O	CO_2	CO_2	H_2O

Therefore, for each $\log p$ and T, the scheme defines a set of η values that are also stored in RRTMG_SW_DATA. Generally, η is defined at 0, 1/8, 2/8,...,1 for the lower atmosphere and 0, 1/4,...,1 for the upper atmosphere. More details regarding the η parameter and the derivation of the absorption coefficients from the LBLRTM model are provided in Mlawer et al. (1997).

In the case of the absorption due to water vapor, three contributions are included. First, the line absorption described above, second the self broadening (i.e. collisions between H_2O molecules) and third, the foreign broadening due to the interaction between H_2O and non-absorbing molecules. The self and foreign broadening are included in RRTMG_SW_DATA. The first one only depends on temperature and it is stored at intervals of 7.2 K from 245.6 to 317.6 K. The second one is defined at four temperatures (i.e. 296, 260, 224 and 188 K) and five pressure levels (i.e. 970, 475, 219 and 3 Pa).

During the code execution, given one value of pressure, temperature and η for a layer, the value for k is fitted using a linear interpolation. Then, the optical thickness at each g-point is evaluated as the sum of three terms: i) the product between k and an effective gas column $u_{1,2}$, ii) the contribution of the minor species and iii) the contribution of self and foreign broadening for water vapor if required.

The effective gas column $u_{1,2}$ is defined as

$$u_{1,2} = u_1 + \frac{S_2}{S_1} u_2. \tag{3.37}$$

The ratio $\frac{S_2}{S_1}$ is also included in RRTMG_SW_DATA.

Minor species are treated as a second order contribution by assuming that the absorption

coefficient is not a function of pressure and temperature.

As there is not documentation regarding the computation of the optical thickness at each band, we will discuss three examples in the following paragraph for illustrating the previous explanation. In order to reduce the nomenclature, the dependence on the g-interval is neglected.

Band 1 As it is shown in Table 3.5, the band between 0.200 and 0.263 μm considers the same key species for lower and upper regions: O_3 and O_2. In this case, the optical thickness is

$$\tau = u_{O_3,O_2} k(T,p,\eta), \tag{3.38}$$

where k is the result of the interpolating the line absorption coefficients to the temperature, pressure and binary specie of the layer. The set of reference k values are different for lower and upper atmospheres.

Band 4 The spectral interval between 0.442 and 0.625 μm shows two different behaviors for each atmospheric region (Table 3.5). In the lower atmosphere, it considers H_2O as key specie and O_3 as minor one. In this case, the optical thickness is evaluated as

$$\tau = u_{H_2O} k_{H_2O}(T,p) + u_{O_3} k_{O_3}. \tag{3.39}$$

As only one key specie is represented, the binary specie parameter is not necessary. Moreover, for this band the broadening effects of water vapor are not considered.

In the upper atmosphere, only ozone is considered as a minor specie. Then, τ is computed as

$$\tau = u_{O_3} k_{O_3}. \tag{3.40}$$

Band 10 In this band, the lower atmosphere includes the contribution of two key species, H_2O and CO_2. Hence, τ is defined as

$$\tau = u_{H_2O,CO_2} k_{H_2O,CO_2}(T,p,\eta) + u_{H_2O}\big(k_{s,H_2O}(T) + k_{f,H_2O}(T,p)\big), \tag{3.41}$$

where, k_s and k_f are the self and foreign absorption coefficients for water vapor.

In the upper atmosphere, only the effect of CO_2 is included and τ is directly,

$$\tau = u_{CO_2} k_{CO_2}(T,p). \tag{3.42}$$

The absorption coefficients stored in RRTMG_SW_DATA are considered as cm^2 molecules^{-1}. Therefore, the optical depth for a dry atmosphere must be expressed previously as molecules cm^{-2}, i.e.

$$u_{dry} = \frac{\Delta p}{g} \frac{A_v}{a_m(1+q_{H_2O})}, \tag{3.43}$$

where A_v is the number of Avogadro (i.e. 6.02·10^{23} mol^{-1}) and a_m is the molecular weight of the moist air defined as

$$a_m = (1-q_{H_2O})a_d + q_{H_2O} a_{H_2O}. \tag{3.44}$$

In Eq. 3.44, a_d and a_{H_2O} are the molecular weight for dry air and water vapor, respectively, taken as 28.966 g mol^{-1} and 18.016 g mol^{-1}.

The optical depth for the other gases is computed as a function of u_{dry} and the mixing ratio q_s of the current specie as

$$u_s = q_s u_{dry}, \tag{3.45}$$

being s H_2O, O_3, CO_2, O_2, CH_4 and N_2O.

Rayleigh scattering

The computation of the Rayleigh scattering is considered for the lower and upper atmospheres and it follows a similar procedure that described for the absorption of the atmospheric gases. Each g-interval has associated one extinction coefficient stored in the auxiliary file RRTMG_SW_DATA. The only exception is in the first and last bands that consider a single extinction coefficient for the entire interval.

Clouds

Optical properties for the cloud droplets are determined following the scheme proposed in Hu and Stamnes (1993). In this parameterization, the radiative fields are evaluated as

$$\frac{\beta_{ext,l}}{LWC} = a_1 r_{e,l}^{b_1} + c_1, \qquad \omega_{0,l} = 1 - a_2 r_{e,l}^{b_2} + c_2, \tag{3.46}$$

$$g_l = a_3 r_{e,l}^{b_3} + c_3, \qquad f_l = g^2. \tag{3.47}$$

The coefficients a_i, b_i and c_i are fitted from the Mie theory using the least-squares method with deviations ∼3% with respect to the theoretic values. These parameters are defined at each spectral interval.

In order to reduce the computational time, these parameters are not computed during the code execution. They are previously evaluated for 58 different values of $r_{e,l}$ and between 2.5 and 60 μm. During the code call, these values are linearly interpolated in terms of the current $r_{e,l}$.

Fig. 3.7 shows that the set of values stored in the code for g and hence, f, have apparently some physical inconsistencies because the values for different $r_{e,l}$ crosses once each others at different wavelengths. In order to explain this issue, we have plotted the original values provided by Hu and Stamnes (1993). As it is shown in Fig. 3.10, this behavior is explained because the values for β_{ext}, ω_0 and

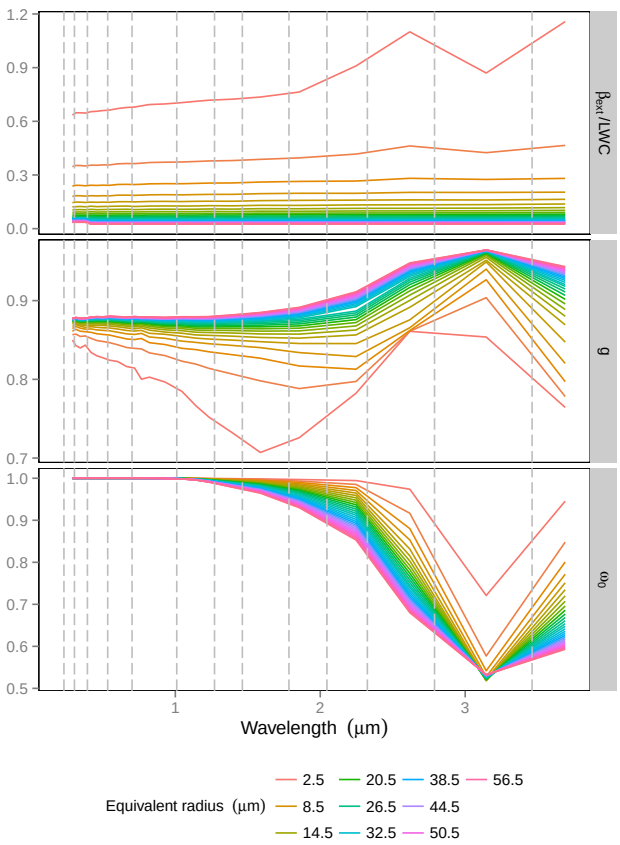

Figure 3.10: Original values of τ, ω_0 and g for cloud droplets provided in Hu and Stamnes (1993). Gray lines indicate the half-width spectral intervals used in RRTMG. f is not included because is just g^2.

g were taken directly at the wavelength intervals used in RRTMG, missing the intermediate information and consequently, producing these strange patterns.

The effective radius for cloud droplets is parameterized in terms of the layer temperature, the snow depth, the land/ocean category and the sea ice fraction in four steps as described in Sect. 3.5.2.

For ice crystals, the scheme has an internal variable called ICEFLAG that controls how this hydrometeor is treated (Table 3.6). The version implemented in the WRF-ARW model uses the option 3 based on Fu (1996). In order to reduce the discussion, only this option will be detailed here.

Table 3.6: Summary of the methods provided for parameterizing ice crystals within the RRTMG code

ICEFLAG	Paper	$r_{e,i}$ range
2	Key (2002),Ebert and Curry (1992)	5–131 μm, >131 μm
3	Fu (1996)	5–140 μm

In ICEFLAG=3, the radiative variables for ice crystals are paramaterized as

$$\frac{\beta_{ext,i}}{IWC} = a_0 + \frac{a_1}{r_{e,i}} \tag{3.48}$$

$$\omega_{0,i} = 1 + b_0 + b_1 r_{e,i} + b_2 r_{e,i}^2 + b_3 r_{e,i}^3 \tag{3.49}$$

$$g_i = c_0 + c_1 r_{e,i} + c_2 r_{e,i}^2 + c_3 r_{e,i}^3 \tag{3.50}$$

$$f_i = d_0 + d_1 r_{e,i} + d_2 r_{e,i}^2 + d_3 r_{e,i}^3 \tag{3.51}$$

Coefficients a_i, b_i, c_i and d_i are obtained from a numerical fitting based on *exact* values derived from a ray-tracing model. Comparing with reference values errors range from 0.3% when θ_0=30° to 2.9% when θ_0=75°.

As in the case of water clouds, $\beta_{ext,i}$, $\omega_{0,i}$, g_i and f_i are evaluated previously for 46 different $r_{e,i}$ between 5 and 140 μm and the spectral intervals. Then, the results are interpolated to the current $r_{e,i}$ value. As it is observed in Fig. 3.8, the set of values stored in the code present serious physical inconsistencies, mostly in the near-IR. In order to explain this behavior, the original values provided by Fu (1996) have been analyzed (Fig. 3.11). On the one hand, the strange patterns observed between spectral bands are a consequence of using directly the values derived from Fu (1996) at RRTMG bands. On the other hand, the values provided by Fu end at 4 μm. Therefore, some error was introduced during the process of extrapolating this data-set to the remaining near-IR bands.

The effective radius for ice crystals is based on Kristjánsson et al. (1999) in terms of the temperature of the layer ad detailed in Sect. 3.5.2.

Finally, these values are δ-scaled to obtain τ' and ω_0' as

$$\tau' = \tau_l + \tau_i \tag{3.52}$$

$$\omega_0' = \frac{\omega_{0,l} + \omega_{0,i}}{\tau'} \tag{3.53}$$

$$g' = \frac{1}{\omega_{0,l} + \omega_{0,i}} \left(\omega_{0,l} \frac{g_l - f_l}{1 - f_l} + w_i \frac{g_i - f_i}{1 - f_i}\right) \tag{3.54}$$

Aerosols

Aerosols are controlled by the option aer_opt from the namelist.input file. Basically, this option enables a flag that drives two different approaches.

When aer_opt is 2 then, the scheme require an input for τ_{aer}, $\omega_{0,aer}$ and g directly by each layer and spectral interval (Sect. 3.2.1). On the contrary, when aer_opt is 1, the scheme requires only τ_{aer} at 550 nm by each layer. This value is extrapolated to the other bands during the code execution considering one or more of 6 ECMWF aerosol types.

Moreover, this scheme can be coupled with the WRF-CHEM working in a similar way that Goddard (Sect. 3.4.2).

When aer_opt is set to 1, RRTMG uses the aerosol climatology derived from (Tegen and Lacis, 1996). This information is stored in three files: aerosol_plev.formatted, aerosol_lat .formatted, aerosol_lon.formatted and aerosol.formatted that must be located in the running folder. The first, second and third files contain information of the pressure levels, latitudes and longitudes, respectively. The last file has the monthly information of the optical depth at 550 nm for 6 species: organic carbon, sea salt, dust, black carbon, sulfate and stratospheric aerosol (i.e. volcanic ashes). The spatial data consists into a grid of 46 latitudes, 72 longitudes and 12 pressure levels.

This information is loaded at the beginning of the simulation and interpolated in time and space at each radiative call. The radiative transfer variables at each spectral interval are determined using internal data-sets stored in a routine called *swaerpr*.

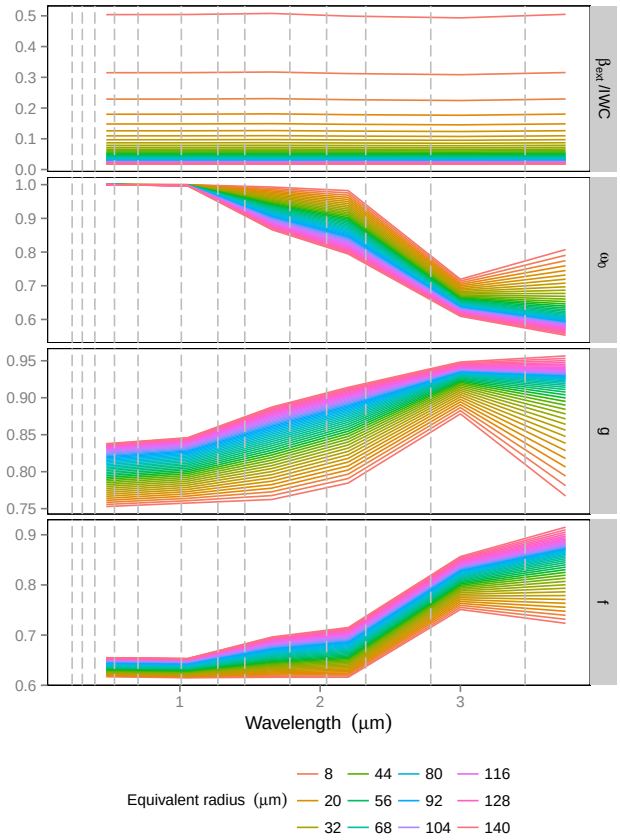

Figure 3.11: Original values of τ, ω_0, g and f for ice crystals provided in Fu (1996). Gray lines indicate the half-width spectral intervals used in RRTMG.

Surface albedo

The scheme can consider different albedos for diffuse and direct components. Generally, they are simplified using the same albedo. However, when the land surface is parameterized with the Simplified Simple Biosphere (SSiB) LSM (Xue et al., 1991; Shufen and Yongkang, 2001), the RRTMG considers different albedos for each component of the flux.

3.6.3 Radiative transfer solver

RRTMG has three modes for solving the RTE equation driven by a variable called kmodts that is fixed inside the code. The default version corresponds to the PIFM approximation (Table 2.2)

proposed by Zdunkowski et al. (1980) with kmodts=2. The other options are the Eddington approximation (Joseph et al., 1976) (i.e. kmodts=1) and the Discrete Ordinates (Liou, 1973) (i.e. kmodts=3). The vertical integration of the fluxes is performed using the adding method (Chap. 2.4).

The scheme parameterizes an extra layer between the TOM and the TOA assuming a constant temperature and trace gases mixing ratio with respect to the last level of the model.

Sub-grid cloud effects are considered using the MCICA (Chap. 2.5.4) following Pincus et al. (2003).

3.6.4 Updates in RRTMG-fast

The RRTMG-fast is an optimized version for RRTMG introduced in the version 3.7 of the mode. As it is indicated in the model website (http://www2.mmm.ucar.edu/wrf/users/wrfv3.7/updates-3.7.html), this new code is compatible with conventional, Intel Xeon Phi processors and Graphics Processor Units (GPUs) based on the CUDA libraries. The option for this scheme corresponds to ra_sw_physics = 24.

3.7 FLG

This scheme is based on the model Fu-Liou-Gu (Gu et al., 2010) that was included in WRF in version 3.4 following the details presented in Gu et al. (2011). At the same time, this scheme is an upgrade version of the original parameterization developed by Fu and Liou (1992, 1993) including the studies of Gu et al. (2003) and Gu et al. (2006). Some of the code implementations are based on the thesis dissertation of Dr. Fu (Fu, 1991).

The scheme works within shortwave and longwave regions of the electromagnetic spectrum. However, only the solar case is analyzed in this chapter.

The FLG parameterization is very customizable inside the code. Nevertheless, these options can only be modified before compiling and hence, it is not available for mainstream users. In this chapter, we will explain the different modes of working describing in depth the settings used in the default version of the WRF model.

3.7.1 Spectral bands

The solar spectrum is divided in six spectral bands: one covering the UV-PAR regions in which the ozone absorption is considered and the other five intervals covering the near-IR considering the water vapor absorption (Table 3.7). For each band, the molecular absorption is evaluated using the CKD method with 54 g-intervals non-uniformly distributed.

Table 3.7: Comparison off the absorbers and scatter at each spectral interval.

Spectral range [μm]	g-intervals	Absorbers/scatters
0.200–0.700	10	O_3, Rayleigh
0.700–1.300	8	H_2O, Rayleigh
1.300–1.900	12	H_2O, Rayleigh
1.900–2.500	7	H_2O, Rayleigh
2.500–3.500	12	H_2O, Rayleigh
3.500–4.000	5	H_2O, Rayleigh

3.7.2 Optical properties

The code includes a flag denoted by NGAS which controls the species considered in the radiative transfer computation. In the default version, NGAS is set to 0 and only the ozone and water vapor are considered. By contrast, when this flag is enabled, the absorption from O_2, CO_2, SO_2, CH_4, NO_2, NO, CH_3 and Chlorofluorocarbons (CFCs) is calculated. However, the effect of these species is not included in the operational version due to the high time consumption by the CKD method.

Water vapor absorption

The absorption due to water vapor is computed using non-uniform g values at each band (Table 3.7). These values are defined as a function of the temperature as

$$\ln k = a \ + b(T - 245) + c(T - 245)^2, \tag{3.55}$$

at eleven pressure levels (i.e. 1000, 631, 398, 251, 158, 100, 63.1, 39.8, 25.1, 15.8 and 10 hPa). At each layer, Eq. 3.55 is evaluated while the dependence with the pressure is derived by a linear interpolation.

Ozone absorption

The ozone absorption is considered in 10 g-intervals in one spectral band.

The version implemented in the model can work with three types of vertical profiles by using a flag in the code denoted as NOZONE:

- For NOZONE=0, the ozone profile is not considered in the radiative transfer computation.
- For NOZONE=1, the scheme considers preescribed ozone profiles
- For NOZONE=2, the scheme could use input profiles derived externally from the radiative package.

The case of NOZONE=2 is not useful because the code is not finished yet. The default case is with NOZONE=1. In this case, the FLG scheme uses the same ozone profiles than Goddard and New Goddard (Fig. 3.6).

Rayleigh scattering

The Rayleigh extinction coefficient is assumed as a constant at each spectral interval. In the first band, the extinction coefficient is computed as a function of μ_0 as

$$k_R = -3.902860 \cdot 10^{-6}\mu_0^2 + 6.120070 \cdot 10^{-6}\mu_0 + 4.177440 \cdot 10^{-6} \tag{3.56}$$

The values for the other bands are derived from Slingo and Schrecker (1982).

At all spectral intervals ω_0 is taken as 1. The expansion coefficients of the phase function necessary for the four-stream approximation (Sect. 2.3.4) are 0, 0.5, 0 and 0, respectively. Therefore, g and f are taken as 0 and 0.1, respectively.

Clouds

The treatment of the cloud overlapping can be selected with the flag NFRACT. When this flag is disabled (by default), binary cloud fractions are considered: i.e. cloudless or overcast. In this case, the overlapping assumption becomes trivially. On the other hand, when NFRACT is enabled, cloud fraction at each layer can be any value between 0 and 1 and the maximum cloud overlapping is applied.

The τ, ω_0 and g for water clouds are parameterized as a function of the LWC and $r_{e,l}$ following Eqs. 2.151, 2.152 and 2.153 but including an additional term in $r_{e,l}^{-3}$ in the first one and $r_{e,l}^{3}$ in the second and third equations. The forward scattering fraction is computed as g^2.

The set of coefficients used in these polynomials are based on Fu (1991). The data-sets stored within the code contains the coefficients for a set of $r_{e,l}$ ranging from 4.18 to 31.23 μm and for LWC between 0.05 to 2.50 gm^{-3} (Fig. 3.7). In a first stage, the τ, ω and g are evaluated at the reference $r_{e,l}$ and LWC data-sets and then, they are interpolated to the layer conditions.

The first two expansion coefficients of the phase function are evaluated as $3g$ and $5f$ from Eqs. 2.26 and 2.66. The other two coefficients are taken as 0.

In practice, $r_{e,l}$ is set to 10 μm and thus, the full potentiality of the described data-set is not actually used.

The computation of the radiative variables for ice crystals is more complex. The treatment of $r_{e,i}$ has four different options controlled by the variable NPDE (Table 3.8). The default version is with NPDE=2.

Table 3.8: Summary of the methods provided for parameterizing $r_{e,i}$ within the FLG code. Options 3 and 4 are related with external data provided by satellite sources. However, the code indicates that these modes have not been really tested.

NPDE	Paper	Variables	$r_{e,i}$ range
0	-	-	85 μm (constant)
1	Gu and Liou (2006)	IWC	10–150 μm
2	Liou et al. (2008)	IWC	10 – 150 μm (default)

Liou et al. (2008) shows an analysis of the correlation between IWC and $r_{e,i}$ for Tropical cirrus, Mid-latitude cirrus and Arctic ice clouds using data-sets from different campaigns. These values are fitted as

$$\ln r_{e,i} = a \ + b \ln IWC + c(T - 245)^2 \tag{3.57}$$

Coefficients a, b and c depend on the regions using 30° and 60° the thresholds for choosing between Tropical, Mid-latitude and Arctic based on the coordinates of each grid-point. In fact, three curves are evaluated: minimum, mean and maximum. The $r_{e,i}$ is computed as a random number between the minimum and the maximum. The final value can not be lower than 10 μm and larger than 150 μm.

The parameterization of the radiative variables is based on a set of polynomials for β_{ext}/IWC, ω_0 and the first four expansion coefficients of the phase function expressed in terms of the $r_{e,i}$. The set of coefficients to be used can be controlled by the internal flag NICE. In total, there are eight different options (Table 3.9). The default configuration of the code uses NICE=2 (Fig. 3.7). Given one value of $r_{e,i}$, each polynomial is evaluated.

Table 3.9: Methods for computing the radiative variables for ice crystals in FLG. Due to the low documentation inside the code, the details provided for all options is not the same.

NICE	Description
0	It uses old coefficients denoted as FLICE93
1	It uses the coefficients provided by Professor Feng Zhang
2	Default. It uses the coefficients provided by Professor Qing Yue
3	Tropical treatment following by using the coefficients provided by Professor Qing Yue
4	Mid-latitude treatment following by using the coefficients provided by Professor Qing Yue
5	It uses coefficients denoted as FLICE95
6	The radiative variables are computed following Yang et al. (2000)
7	The radiative variables are computed following Yang et al. (2005)

Aerosols

The code has a flag called NAERO for choosing the aerosol treatment. When this flag is set to 0, aerosols are not considered. This is the default version in the WRF-ARW model. When NAERO=1, aerosols from preescribed profiles are considered. Finally, when NAERO is set to 2, aerosols can be provided externally.

The preescribed aerosols consist in 18 different types of aerosols derived from the Aerosols and Clouds (OPAC) data-base (D'Almedia et al., 1991; Tegen and Lacis, 1996; Hess et al., 1998).

Surface albedo

The surface albedo is simplified into a single value provided by the static data of the WRF-ARW model.

3.7.3 Radiative transfer solver

At each level the transmissivity and the reflectivity is evaluated using the δ-four-stream approximation (Sect. 2.3.4). The interaction between layers due to the multiscattering events is not considered in this scheme as indicated in Sect. 2.4. This scheme considers the layer between the TOM and the TOA as transparent.